# Helium in One-Dimensional Nanopores: Free Dispersion, Localization, and Commensurate/Incommensurate Transitions with Nonrigid Orbitals

Massimo Boninsegni,[1] Seung-Yeop Lee,[2] and Vincent H. Crespi[2]
[1]*Department of Physics, San Diego State University, San Diego, California 92182*
[2]*Department of Physics, 104 Davey Laboratory, Penn State University, University Park, Pennsylvania 16802-6300*
(Received 2 December 2000)

The single-particle states of helium within a bundle of carbon nanotubes can range from nearly free-particle dispersion to localization, even within a single bundle. At intermediate effective masses, the corrugation in the external potential can be comparable to the intrasite He-He hard-core interaction. This results in a commensurate/incommensurate transition, where the mobility of the doubly occupied domain-wall solitons at high density greatly exceeds the corresponding hole mobility below the transition.

DOI: 10.1103/PhysRevLett.86.3360 PACS numbers: 67.90.+z, 67.20.+k, 67.40.–w, 68.65.–k

Recent advances in materials synthesis hold the prospect of producing hosts in which adsorbed helium (He) atoms form a strictly one-dimensional (1D) system, immersed in a background potential that can be tuned over a range of amplitudes and periods, including even quasiperiodic potentials. Specifically, we refer to 1D nanoporous substrates such as bundles of carbon nanotubes [1], wherein He atoms can be bound in the interstitial channels or within the tubes themselves [2,3]. These experimental realizations could provide a unique opportunity to access exactly solvable models of many-body quantum dynamics. Such investigations are predicated on an understanding of the single-particle properties of the active species. Here we demonstrate that the single-particle properties of $^4$He in carbon nanotube bundles can vary over an enormous range, from nearly free-particle dispersion in tube interiors and short-period interstitial channels to millionfold enhancements of the effective mass in longer-period channels. In between these two limits, the competition between the external potential and the He-He hard-core interaction can induce an incommensurate-commensurate transition, with broken particle-hole symmmetry about single filling of the adsorption sites.

Single-walled carbon nanotubes of typical diameter $\sim$1.4 nm self-organize into bundles of 1 to 100 tubes in a triangular lattice. For such systems, the tube interiors and the 1D interstitial channels within the bundle can form strongly attractive substrates for adsorbed He (although impurities and agglomerations of adsorbates on tube openings could impede access to some adsorption sites [4]). Adsorbates such as He could form 1D quantum systems which occupy a regime very different from that of the on-tube electronic states [5]. Previous studies showed how weak interchannel interactions could induce condensation of He within ordered bundles and briefly noted the extension to less well-ordered systems [6]. Here, we study the single-channel dynamics of $^4$He across the range of heterogeneous systems that likely exist in current experimental samples. We begin by calculating the single-particle states and use these results to design model potentials for subsequent many-body calculations. The potential is constructed from a superposition of Lennard-Jones pair interactions between the He atom and the surrounding carbon atoms [2], either those in the three tubes bordering an interstitial channel or, for states inside a single tube, the atoms of the surrounding tube. We solve Schrödinger's equation for the adsorbed $^4$He using a plane wave axial basis, and Laguerre or Bessel polynomials to describe the transverse confinement. First we examine the case where each of the three tubes bordering an interstitial channel has the same wrapping indices: (10, 10):(10, 10):(10, 10), (17, 0):(17, 0):(17, 0), and (12, 6):(12, 6):(12, 6) [7]. Later we examine states within intersitial channels formed from tubes of different wrapping indices, as well as within the core of a single tube (using the Bessel function basis in this case).

For the homogeneous systems, the single-particle dispersion is a sensitive function of the relative axial alignment of the three tubes that define a single channel (see Table I). When the tubes are perfectly aligned, the potential barrier impeding axial movement of He is highest, on the order of 20 K. These configurations yield the largest effective mass. When the tubes are out of alignment, the potential barrier can decrease substantially due to cancellations between the contributions of neighboring tubes, yielding $m^* \approx m$. For the chiral (12, 6):(12, 6):(12, 6)

TABLE I. Lowest-band effective mass enhancement $m^*/m$ for $^4$He in various tube bundles. The range of values for the interstitial channels reflects changes in the intertube axial offsets for the three tubes bordering the channel.

| Interstitial channel | $m^*/m$ |
|---|---|
| (10, 10):(10, 10):(10, 10) | $1 \leftrightarrow 1.3$ |
| (17, 0):(17, 0):(17, 0) | $1 \leftrightarrow 16$ |
| (12, 6):(12, 6):(12, 6) | $1 \leftrightarrow 10^7(\infty)$ |
| (16, 1):(16, 1):(11, 8) | $\infty$ |
| (11, 8):(16, 1):(15, 3) | $\infty$ |
| **Tube interiors** | $m^*/m$ |
| (17, 0) | 1.0 |
| (10, 10) | 1.0 |
| (12, 6) | 1.4 |

 0031-9007/01/86(15)/3360(4)$15.00 

interstitial channel, the lowest few bands under perfect axial alignment are nearly dispersionless, with an interband separation of $\sim 10$ K.

In the moderate-to-high mass regime, the dispersion is governed by the weak overlap between adjacent axial binding sites and so is sensitive to changes in overlap due to variations in the intertube separation. For example, increasing the intertube separation from 3.3 to 3.4 Å in a $(17, 0)$:$(17, 0)$:$(17, 0)$ bundle reduces the maximal effective mass enhancement from 16 to 8. Since the sets of tubes given in Table I have slightly different diameters, we recalculated the effective mass for helium in a $(12, 6)$ interstitial channel with a slight (0.87%) dilation in bundle lattice constant which brings the channel width to a value midway between that of the $(17, 0)$ and $(10, 10)$ bundles (which differ by only 0.5%). The effective mass changes only very slightly, indicating that the large variations in effective mass observed across the ranges of tubes studied arise primarily from the variations in axial alignments and wrapping angles.

Bundles likely contain a mixture of different tube wrapping angles. In such a heterogeneous system, the interstitial channel can be quasiperiodic, since the axial unit cells of arbitrary tubes are usually incommensurate. If we exclude trivial commensurations such as $(12, 6)$:$(14, 7)$ and $(17, 0)$:$(18, 0)$, then very few commensurate cases remain, all with very long axial periods. We make this problem tractable from a band structure standpoint by choosing a set of three nearly commensurate tubes and then slightly stretching or shrinking the constituents until perfect commensuration is achieved. Very slight ($\sim 1\%$) extensions or contractions can make the axial period manageably small, with only a minor perturbation to the potential (albeit one that removes quasiperiodicity). As we shall see, much of the physics in these cases occurs within a single unit cell, so that the artificial periodicity that we impose for computational convenience is not a major concern, so long as one keeps in mind that the interesting longer-range consequences of quasiperidicity are lost.

We examine two specific cases: channels bounded by $(16, 1)$:$(16, 1)$:$(11, 8)$ and $(11, 8)$:$(16, 1)$:$(15, 3)$ nanotubes. These systems show uniformly large lowest-band effective masses that are essentially infinite (i.e., greater than $\sim 10^6$). The effective mass is independent of the axial registry between tubes, because a nearly incommensurate system such as this already samples over a dense mesh of local intertube registries within a single unit cell. Curiously, it is the *heterogeneous* bundle that is homogeneous under relative axial shifts. Such shifts are likely to occur in experimental bundles, since they are typically not perfectly straight.

These single-particle results can be synthesized within a simple toy model that captures much of the essential physics. Figure 1 shows the isocurves of constant effective mass in a simple sinusoidal potential of variable amplitude and period. We identify the four classes of interstitial channels [i.e., short-period homogeneous $(n, n)$ and $(n, 0)$, long-period homogeneous, and long-period heterogeneous] with successive regions $A$, $B$, $C$, $D$ of the isosurface plot. Vertical motion on the plot corresponds to changing the amplitude of the potential as if varying the intertube axial offsets. As expected, $m^*$ and its range of variation grow rapidly as the periodicity increases. This simple model demonstrates that the high effective masses arise from the potential barriers that can form within a single long-period unit cell, as expected in a periodic approximate to Anderson localization.

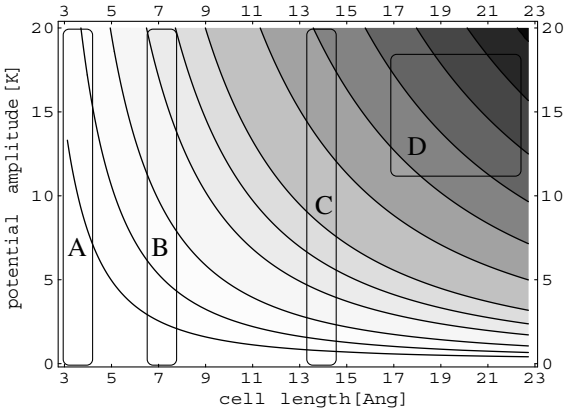


FIG. 1. The ratio of the effective mass of $^4$He to the free mass as a function of amplitude and period of a model sine-function 1D potential. The contour lines have values 1.1, 1.5, 3, 10, 30, 100, $10^3$, $10^4$, $10^5$, $10^6$, $10^7$, $10^8$ from the left bottom to the right top. Regions $A$, $B$, $C$, and $D$ model (crudely) the four classes of channels discussed in the text. Isocurves are functions of (amplitude) (period)$^2$.

The highly localized states in heterogeneous bundles contrast sharply with nearly free-particle dispersion within the cores of individual tubes themselves. The intratube states for $(17, 0)$, $(10, 10)$, and $(12, 6)$ nanotubes yield lowest-band effective masses of 1.0, 1.0, and 1.4, respectively, consistent with the effective mass of helium on graphite [8]. The slightly higher effective mass inside the $(12, 6)$ tube reflects its longer axial unit cell. The sharp contrast between intratube and interstitial channel dispersion indicates that a typical bundle contains distinct 1D substrates for He that can have vastly different single-particle properties. In addition, the interaction between He atoms within a single nanotube core can vary in softness depending on the diameter of the tube. Since recent experiments have succeeded in producing tubes of very small diameter [9], we have also calculated the effective masses inside $(7, 0)$, $(4, 4)$, and $(6, 3)$ tubes (in smaller-diameter tubes the overall interaction potential is not binding), obtaining $m^* = 5.9$, 1.0, and 1.0, respectively, at binding energies of $-230$, $-150$, and $-470$ K. The larger effective mass in the $(7, 0)$ tube results from coherent contributions around the tube circumference in a system with moderate unit cell length; the $(6, 3)$ tube, in contrast, shows efficient helical averaging to the potential.

The tight transverse confinement in an interstitial channel favors axial nodes for the lowest few bands and freezes out the transverse degrees of freedom below roughly 10 K.

The confinement of the dynamics to the axial direction justifies the construction of a purely 1D effective potential as a tractable starting point for diffusion Monte Carlo (DMC) calculations of the many-body $^4$He ground state. We can identify three distinct regimes defined by the single-particle effective masses. For $m^* \approx 1$, the system behaves as an ensemble of 1D bosons in a smooth potential. The long unit cell systems with $m^* \to \infty$ lie in the opposite limit of strong disorder and localized states, at least at low density. We focus here on the intermediate regime, wherein the effective mass enhancement is a few-fold. This regime is realized in systems with relatively short axial unit cells, wherein the height of the axial potential barrier tends to be comparable to the He-He hard-core interaction across the width of a typical local minimum in the external potential.

As an archetype for this regime, we construct a 1D potential with a periodic sum of Gaussians $U(z) = A\exp[-z^2/2\sigma^2]$ with height $A = 17.6$ K, width $\sigma = 0.452$ Å, and spacing $a = 4.26$ Å, [i.e., the cell length of an $(n, 0)$ tube]. These parameters give $m^* \approx 2$ for the lowest band with a realistic band separation (qualitatively similar results are expected across a range of parameter values). The DMC calculation using this potential treats $N$ $^4$He atoms of mass $m$ in one dimension with periodic boundary conditions. The microscopic Hamiltonian is

$$\hat{\mathcal{H}} = -\frac{\hbar^2}{2m}\sum_i \frac{\partial^2}{\partial z_i^2} + \frac{1}{2}\sum_{i\neq j} V(z_{ij}) + \sum_{i,l} U(z_i + la), \tag{1}$$

where $z_{ij} = |z_i - z_j|$, $z_i$ being the coordinate of the $i$th $^4$He atom. $V$ is the Aziz He pair potential [10]. Substrate-induced three-body and higher terms in the van der Waals interaction could modify the detailed form of the effective He-He interaction, but the qualitative effects described below depend predominately on the short-range hard-core interaction, which is essentially unaffected by the presence of the substrate. The last term of (1) is the periodic external potential. We use the following variational wave function:

$$\Psi = \exp\left\{-\sum_{i<j} u(z_{ij}) - \sum_{i,l} v(|z_i - la|)\right\}, \tag{2}$$

where $u$ and $v$ have the form $f(z) = \alpha/(1 + \beta z^\mu)$. We simulate densities in the range $0 \le \rho \le 0.4$ Å$^{-1}$; the variational parameters $\alpha$, $\beta$, and $\mu$ (for both $u$ and $v$) were optimized to yield the lowest energy estimate at each density.

Unbiased estimators were used for all quantities. Although the wave function (2) breaks translational invariance, on account of the corrugation, it preserves permutational symmetry among $^4$He atoms. This symmetry, absent in the Jastrow-Nosanow wave functions commonly adopted in DMC simulations of quantum solids, is essential in order to study superfluidity, which depends on the indistinguishability of $^4$He atoms.

The system undergoes a $T = 0$ commensurate to incommensurate phase transition when the He wave function changes from single to higher site occupancy. At low density, the main contribution to the energy $e(\rho)$ comes from the long-range attraction of He atoms. Since particles occupy well-separated potential wells, the hard-core interparticle repulsion has little effect. The sharp break in the sign and magnitude of the slope of $e(\rho)$ at $\rho \approx 0.235$ Å$^{-1}$ (see Fig. 2) reflects the onset of hard-core repulsion in doubly occupied sites. When a site is doubly occupied, the hard-core repulsion within its confines induces a significant spread in the local He wave function. Figure 2 also shows the local density of $^4$He, $\rho_m$, at maxima in the 1D potential, (i.e., the minimal helium density in between adjacent binding sites). The sharp rise at the onset of double occupancy signals a much higher effective intersite hopping rate of the double-occupied domain wall above $\rho \approx 0.235$ Å$^{-1}$, as compared to that of the occupation hole at lower densities. The calculation assumes a perfect lattice translational symmetry, so that the double occupancy is smeared over the entire system; introduction of a localized perturbation could pin the domain walls.

The transition can also be seen in the $^4$He pair correlation function $g(z)$, shown in Fig. 3 at three different densities near the transition. At $\rho \le 0.23$ Å$^{-1}$, the pair correlation function reflects the periodicity of the external potential, whereas, at $\rho \ge 0.3$ Å$^{-1}$, it is scarcely distinguishable from that of free 1D $^4$He [11]. At $\rho = 0.27$ Å$^{-1}$, the pair correlation function shows beats between the competing periodicities.

Figure 2 also gives the $^4$He superfluid density [12] $\rho_S$ as a function of the total $^4$He density inside the channel. This quantity was evaluated by DMC as [13]

$$\rho_S = \rho\left\{\lim_{\tau\to\infty}\left\langle\frac{[\mathbf{R}(\tau) - \mathbf{R}(\mathbf{0})]^2}{2\Lambda\tau}\right\rangle\right\}, \tag{3}$$

where $\langle\ldots\rangle$ is the ground state expectation value, $\mathbf{R}(\tau)$ is the position of the center of mass of the $^4$He many-body system at imaginary time $\tau$, and $\Lambda = \hbar/2Nm$. As the $^4$He density increases from zero, $\rho_S$ initially increases slowly but then decreases as the system approaches the commensurate/incommensurate transition

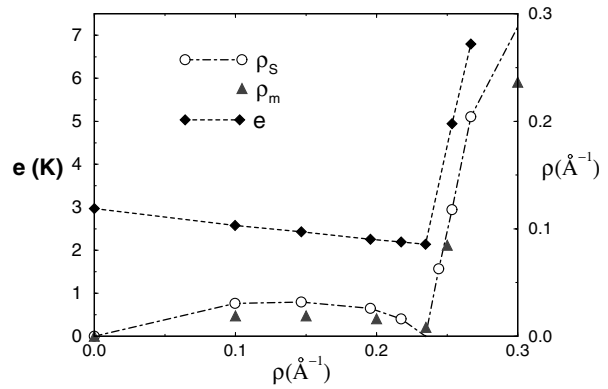


FIG. 2. Binding energy per $^4$He atom $e(\rho)$ within the corrugated channel. The right-hand scale gives the $^4$He superfluid density $\rho_S$ and the local He density $\rho_m$ at maxima of the corrugation potential. Below $\rho \approx 0.23$ Å$^{-1}$ there is less than one particle per site. DMC error bars are smaller than the symbol size.

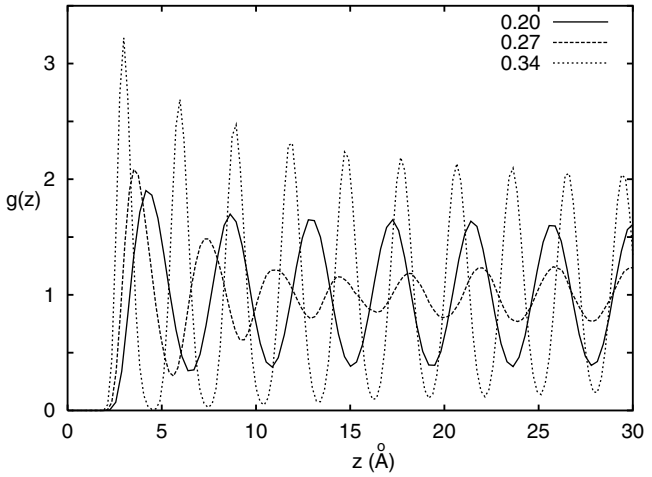


FIG. 3. Pair correlation function $g(z)$ for two He atoms along the channel, computed by DMC at different densities. Error bars of $g(z)$ are omitted for clarity; statistical uncertainties on $g(z)$ are typically of order 0.01 or smaller.

($\rho \sim 0.235$ Å$^{-1}$), where $\rho_S$ vanishes. At higher densities, $\rho_S$ rapidly increases. The strong asymmetry in slope between opposite sides of the commensuration again reflects a lack of particle-hole symmetry around single filling. The loss of superfluidity at commensuration is similar to the superfluid staircases in layered $^4$He films on graphite [14,15].

Mott-Hubbard models for adsorbed He have been proposed for finite ($\sim$10-particle) rings of He within ring-shaped potential minima in certain zeolites [16] and in $^4$He films on graphite [15]. Here, the hard-core interaction within the tight confines of a single lattice site induces substantial change in the underlying single-particle orbitals and thereby violates a standard approximation of the Hubbard model, that the bare hopping rate is independent of site occupancy. The situation is distinct from the familiar multiband Hubbard model, as double occupancy here does not correspond to the occupation of a specific higher band, but rather to a complex superposition of higher-band single-particle basis states. The latter is more simply described in terms of a site-occupancy-dependent hopping rate, with a loss of particle/hole symmetry around single filling. The electronic Hubbard model might also be rendered more realistic, in some cases, through an occupation dependence of the underlying orbital structure and hopping rate.

Although the DMC calculation treated only the single case of $m^* \approx 2$, much of the underlying physics is generic. The dramatic enhancement in the axial mobility of density perturbations with increasing coverage is expected to apply also for heterogeneous systems with higher single-particle effective masses. The mobility of density perturbations could be tuned over a wide range through the influence of the *hard-core* interactions, as opposed to the more familiar delocalization via long-range screening of the Coulomb interactions in electronic systems. These effects are not necessarily restricted to carbon nanotube bundles. Recently developed large-pore zeolites and slightly larger-scale MCM-41 porous silicates [17] provide additional materials systems wherein the pore diameter and corrugation could be tuned to obtain a 1D substrate for He adsorption. The bare walls in such systems are typically highly corrugated and localize the first layers of adsorbed He. However, the range of pore/adsorbate combinations available suggests that one might find a preplating absorbate in a channel of appropriate size, so that the preplated dead layer softens the corrugation in the external potential and surrounds a central channel occupied by 1D He of variable $m^*$.

We acknowledge the NSF for Grants No. DMR-9876232 and No. DMR-9802803 and the Petroleum Research Fund of the ACS for Grants No. 33824-G5 and No. 34778-GB6. We also acknowledge support from the National Partnership for Advanced Computational Infrastructure and from Compaq Computers.

[1] S. Iijima, Nature (London) **354**, 56 (1991); A. Thess *et al.,* Science **273**, 483 (1996).
[2] G. Stan, M. Boninsegni, V. H. Crespi, and M. W. Cole, J. Low Temp. Phys. **113**, 447 (1998).
[3] W. Teizer, R. B. Hallock, E. Dujardin, and T. W. Ebbesen, Phys. Rev. Lett. **82**, 5305 (1999).
[4] S. Talapatra, A. Z. Zambano, S. E. Weber, and A. D. Migone, Phys. Rev. Lett. **85**, 138 (2000).
[5] Y. A. Krotov, D.-H. Lee, and S. G. Louie, Phys. Rev. Lett. **78**, 4245 (1997); L. Balents and R. Egger, Phys. Rev. Lett. **85**, 3464 (2000); C. Kane, L. Balents, and M. P. A. Fisher, Phys. Rev. Lett. **79**, 5086 (1997).
[6] M. W. Cole, V. H. Crespi, G. Stan, C. Ebner, J. M. Hartman, S. Moroni, and M. Boninsegni, Phys. Rev. Lett. **84**, 3883 (2000).
[7] Tube indices express the circumference in lattice coordinates, e.g., R. Saito, M. Fujita, G. Dresselhaus, and M. S. Dresselhaus, Appl. Phys. Lett. **60**, 2204 (1992).
[8] W. E. Carlos and M. W. Cole, Phys. Rev. B **21**, 3713 (1980).
[9] H. Y. Peng *et al.,* Appl. Phys. Lett. **77**, 2831 (2000); L.-C. Qin *et al.,* Nature (London) **408**, 50 (2000); N. Wang *et al., ibid.* **408**, 50 (2000); L.-M. Peng *et al.,* Phys. Rev. Lett. **85**, 3249 (2000).
[10] R. Aziz *et al.,* J. Chem. Phys. **70**, 4330 (1979).
[11] M. Boninsegni and S. Moroni, J. Low Temp. Phys. **118**, 1 (2000).
[12] Pure 1D systems are subject to the effects of, e.g., localized imperfections that can subdivide the system and affect the experimental signatures of superfluidity.
[13] E. L. Pollock and D. M. Ceperley, Phys. Rev. B **36**, 8343 (1987).
[14] P. A. Crowell and J. D. Reppy, Phys. Rev. Lett. **70**, 3291 (1993).
[15] G. T. Zimanyi, P. A. Crowell, R. T. Scalettar, and G. G. Batrouni, Phys. Rev. B **50**, 6515 (1994).
[16] B. Y. Chen, S. D. Mahanti, and M. Yussouff, Phys. Rev. Lett. **75**, 473 (1995).
[17] D. E. W. Vaughan and K. G. Strohmaier, U.S. Patent No. 5,455,020 (1995); C. T. Kresge, M. E. Leonowicz, W. J. Roth, J. C. Vartuli, and J. S. Beck, Nature (London) **359**, 710 (1992).